Chemical Science

ROYAL SOCIETY OF CHEMISTRY

EDGE ARTICLE

View Article Online
View Journal | View Issue

Check for updates

Cite this: *Chem. Sci.*, 2024, **15**, 3545

All publication charges for this article have been paid for by the Royal Society of Chemistry

A polydopamine coating enabling the stable cycling of MnO_2 cathode materials in aqueous zinc batteries†

Guoli Zhang,[a] Jiaqi Zhu,[a] Lu Lin,[a] Yaozhi Liu,[a] Shuo Li,[a] Qianrui Li,[a] Xiao-Xia Liu *[abc] and Xiaoqi Sun *[ab]

Received 14th November 2023
Accepted 16th January 2024

DOI: 10.1039/d3sc06096a

rsc.li/chemical-science

MnO_2 is a desired cathode candidate for aqueous zinc batteries. However, their cycling stability is seriously limited by active material dissolution, and pre-addition of Mn^{2+} salts in electrolytes is widely required to shift the dissolution equilibrium. Herein, we synthesize a polydopamine (PDA) coated MnO_2 composite material (MnO_2/PDA) to realize stable cycling in zinc cells without relying on pre-added Mn^{2+}. The functional groups on PDA exhibit strong coordination ability with the Mn active material. It not only confines dissolved species within the cathode during discharge, but also enhances their deposition back to the cathode during charge to retrieve the active material. Thanks to this effect, the cathode achieves 81.1% capacity retention after 2000 cycles at 1 A g^{-1} in the 1 M $ZnSO_4$ electrolyte, superior to 37.3% with the regular MnO_2 cathode. This work presents an effective strategy to realize the stable cycling of manganese oxide cathode materials in aqueous zinc batteries.

Introduction

Rechargeable aqueous zinc batteries have attracted great attention for their low cost, high safety and environmental friendliness.[1–10] Zn metal is applied as the anode, providing a high capacity of 820 mA h g^{-1}/5855 mA h cm^{-3} and low redox potential.[11–13] So far, the main cathode families studied for Zn batteries include Mn-based oxides, V-based oxides, polyanion materials and organic compounds.[14–16] Among them, manganese oxides show great promise due to their high capacity, relatively high voltage and simple preparation.[17] Various crystal structure control, morphology engineering and composite design methods have been applied to enhance the capacity and rate capability. Meanwhile, MnO_2 has been revealed to undergo complicated energy storage processes in aqueous zinc cells, including the de/intercalation of Zn^{2+} and/or H^+, conversion reactions, and dissolution–deposition reactions.[18,19]

One of the most important limiting factors of manganese oxide cathode materials in zinc batteries is rapid capacity fading, which is caused by active material dissolution.[20,21] The main and most effective strategy for inhibiting dissolution and promoting cycling stability is to shift the dissolution equilibrium by adding extra Mn^{2+} in electrolytes.[22–25] Besides, it is proposed that the introduction of pillars, *e.g.*, polyaniline and water, in layered MnO_2 enhances its structural stability and improves capacity retention.[26] In addition, heteroatom doping and compositing with conductive compounds[27,28] have been reported to improve the electrochemical stability of MnO_2. Nevertheless, the majority of MnO_2 studies still rely on pre-added Mn^{2+} salts in electrolytes to achieve reasonable cycling performance.

A possible concern for Mn^{2+} additives, on the other hand, is that they would be oxidized and deposited at the cathode during the charge process,[29,30] functioning as extra active materials. Therefore, the tests of MnO_2 in electrolytes free of pre-added Mn^{2+} would reflect the cycling performance of the cathodes themselves. In addition to suppressing dissolution, an effective strategy to realize stable cycling would be the recycling of dissolved active material. This can be realized by promoting the deposition of dissolved Mn^{2+} back to the cathode and oxidation to MnO_2 during the charge process. In order to achieve this goal, we herein construct a polydopamine (PDA) coated MnO_2 composite material (MnO_2/PDA). Specifically, PDA contains various active sites to coordinate with the Mn active material. It not only interacts with and confines dissolved active material at the cathode during discharge, but also facilitates the back-deposition of dissolved Mn^{2+} during charge. A stable long-term cycling of the MnO_2/PDA composite material is thus realized. It retains 147 mA h g^{-1} capacity after 2000 cycles at 1 A g^{-1} in the $ZnSO_4$ electrolyte free of Mn^{2+} additives, corresponding to 81.1% capacity retention, superior to only 90 mA h g^{-1} capacity left (37.3% retention) for the bare MnO_2 material.

[a]*Department of Chemistry, Northeastern University, Shenyang 110819, China. E-mail: xxliu@mail.neu.edu.cn; sunxiaoqi@mail.neu.edu.cn*

[b]*National Frontiers Science Center for Industrial Intelligence and Systems Optimization, Northeastern University, 3-11 Wenhua Road, Shenyang, 110819, China*

[c]*Key Laboratory of Data Analytics and Optimization for Smart Industry (Northeastern University), Ministry of Education, China*

† Electronic supplementary information (ESI) available. See DOI: https://doi.org/10.1039/d3sc06096a

Results and discussion

The standard MnO_2 material was obtained by a hydrothermal reaction. To achieve a PDA coating, an *in situ* self-polymerization of dopamine was further carried out. Fig. 1a compares the X-ray diffraction (XRD) patterns of MnO_2 and MnO_2/PDA. Both patterns are well fitted to the alpha-phase MnO_2 (JCPDS: 44-0141),[31] suggesting that the coating does not affect the crystal structure of MnO_2. The morphology and microstructure of the MnO_2/PDA composite are characterized. The scanning electron microscopy (SEM) image shows a nano-rod morphology with micron-length and a diameter below 100 nm, which resembles that of the original MnO_2 (Fig. 1b and S1†). Fig. 1c shows the high-resolution transmission electron microscopy (HR-TEM) image. Well-resolved lattice fringes with a spacing of 0.51 nm are present in the inner part of the nano-rods, corresponding to the (200) plane of α-phase MnO_2. Meanwhile, an amorphous layer with a thickness below 2 nm is identified on the surface. The energy dispersive X-ray spectroscopy (EDS) elemental mapping reveals the uniformly distributed Mn, C, and O on the nano-rods (Fig. 1d). This confirms that the amorphous PDA layer is homogeneously coated on the surface of MnO_2.

The composition of MnO_2/PDA is further studied. Fig. 1e shows the Fourier transform infrared spectroscopy (FT-IR) spectra of PDA and MnO_2/PDA. The characteristic vibrations of PDA are shown in the composite material, including that of C–N at 1382.4 cm^{-1}, C=O at 1680.6 cm^{-1}, and N–H/O–H in the range of 3000 cm^{-1} to 3400 cm^{-1}. Interestingly, these vibrations experience a redshift in comparison to those of bare PDA. Meanwhile, the Mn–O vibration in MnO_2/PDA shows up at 633.3 cm^{-1} in the Raman spectrum, which is blueshifted compared to that at 630.8 cm^{-1} in bare MnO_2 (ref. 32 and 33) (Fig. 1f). These changes suggest the coordination between MnO_2 and PDA at the interface and confirm their strong interactions in the composite material.[34,35] Fig. 1g–i and S2† show the X-ray photoelectron spectroscopy (XPS) spectra of MnO_2/PDA. The C–N peak is identified at 399.8 eV in the N 1s spectrum, and C–O and C=O components are found at 531.2 eV and 532.7 eV in the O 1s spectrum, respectively [36] These species are

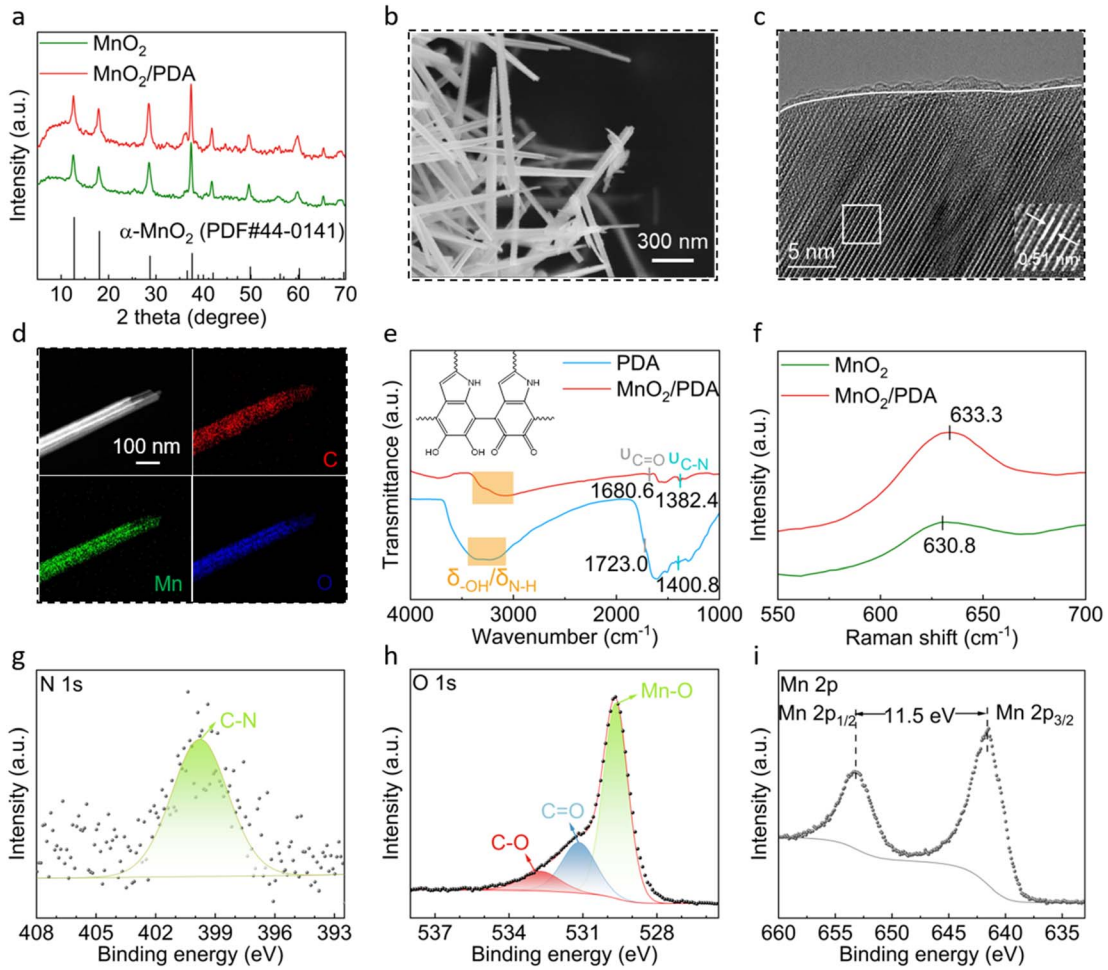

Fig. 1 (a) XRD patterns of MnO_2 and MnO_2/PDA. (b) SEM image, (c) HR-TEM image and (d) EDS mapping of MnO_2/PDA. (e) FT-IR of PDA and MnO_2/PDA (inset shows the chemical structure of PDA). (f) Raman spectra of MnO_2 and MnO_2/PDA. (g) N 1s, (h) O 1s, and (i) Mn 2p XPS of MnO_2/PDA.

also present in the C 1s spectrum. Besides, a third O peak is revealed at 529.7 eV in the O 1s spectrum. This corresponds to the lattice oxygen in MnO_2. In the Mn 2p spectrum, the splitting energy between the $2p_{3/2}$ and $2p_{1/2}$ peaks is 11.5 eV, which matches well with that of the typical MnO_2 material.[37–39] Thermogravimetric analysis (TGA) is performed for the MnO_2/PDA composite. As shown in Fig. S3,† the decomposition of PDA takes place after 300 °C, and its weight percent is estimated to be 12%. The molecular weight of PDA is measured to be 1105 with a polydispersity of 3.8 by gel permeation chromatography (GPC).

The electrochemical performance of MnO_2 and MnO_2/PDA cathode materials is studied in zinc cells. The 1 M $ZnSO_4$ aqueous solution free of Mn^{2+} additives is applied as the electrolyte to evaluate the stability of the cathodes themselves. Galvanostatic charge and discharge is first carried out at a relatively low current density of 0.1 A g^{-1}. As shown in Fig. 2a, the MnO_2 cathode delivers a capacity of 323 mA h g^{-1} in the first cycle, but it decays significantly in subsequent cycles. Only 222 mA h g^{-1} capacity is left after 100 cycles. This poor cycling stability is typical for regular MnO_2 cathode materials in aqueous zinc cells, resulting from irreversible active material dissolution. In comparison, the MnO_2/PDA cathode presents much improved stability. The capacity drops slowly from 300 mA h g^{-1} to 265 mA h g^{-1} over 100 cycles (Fig. 2b and S4†). The rate performance is studied for the two cathodes (Fig. 2c–e). The MnO_2 cathode again experiences capacity decay at various current densities, and it is more serious at lower current densities. This is attributed to the longer time for the dissolution process at slower rates. Only 92 mA h g^{-1} capacity is left upon the increase of current density to 2 A g^{-1}, and a poor capacity of 224 mA h g^{-1} is recovered with the decrease of current density back to 0.1 A g^{-1}. The MnO_2/PDA cathode material, in contrast, presents stable capacity retentions at different current densities. The capacities of 278, 257, 220, 164 and 134 mA h g^{-1} are obtained at 0.2, 0.3, 0.5, 1 and 2 A g^{-1}, respectively. With the return of current density to 0.1 A g^{-1}, a high capacity of 304 mA h g^{-1} is still retained.

Long-term cycling is carried out at 1 A g^{-1} (Fig. 2f). The MnO_2/PDA cathode again presents better cycling performance. The capacity undergoes a short degradation period followed by a gradual increase in subsequent cycles. Considering the complicated energy storage processes of the MnO_2 active material, including one electron transfer and two electron transfer as well as irreversible dissolution of Mn^{2+} in the electrolyte, repeated cycles are required for the stabilization of these processes.[40] The capacity finally reaches 147 mA h g^{-1} after 2000 cycles, which is 81.1% that of the initial cycle. This is superior to the MnO_2 cathode, with fast capacity decay during early cycles (Fig. S5†) and only 90 mA h g^{-1} capacity retained after 2000 cycles. The above analysis demonstrates the largely improved electrochemical performance of the MnO_2 cathode material in aqueous zinc cells with the help of a PDA coating.

Electrochemical impedance spectroscopy (EIS) is carried out for the MnO_2 and MnO_2/PDA electrodes to study the reaction kinetics. Fig. 3a compares the Nyquist plots at 25 °C. It reveals a charge transfer resistance (R_{ct}) of 24 ohm for MnO_2, which largely reduces to 10 ohm for MnO_2/PDA. EIS is then performed at various temperatures. As shown in Fig. 3b and c, the semicircles of MnO_2/PDA all exhibit smaller radii to the ones of MnO_2, suggesting the smaller charge transfer resistance of the former at different temperatures. The activation energy (E_a) is further calculated from the linear fits of $\ln(R_{ct}^{-1})$ *versus* $1/T$ plots according to the Arrhenius equation (Fig. 3d). The activation energy of the MnO_2/PDA cathode is calculated to be 32.8 kJ mol^{-1}, which is lower than 40.9 kJ mol^{-1} of the MnO_2 cathode. This suggests that the reaction kinetics of the MnO_2 material is effectively enhanced with the help of a PDA coating. This is attributed to the facilitated desolvation process of Zn^{2+} and H^+ by PDA, which coordinates with Zn^{2+} and forms

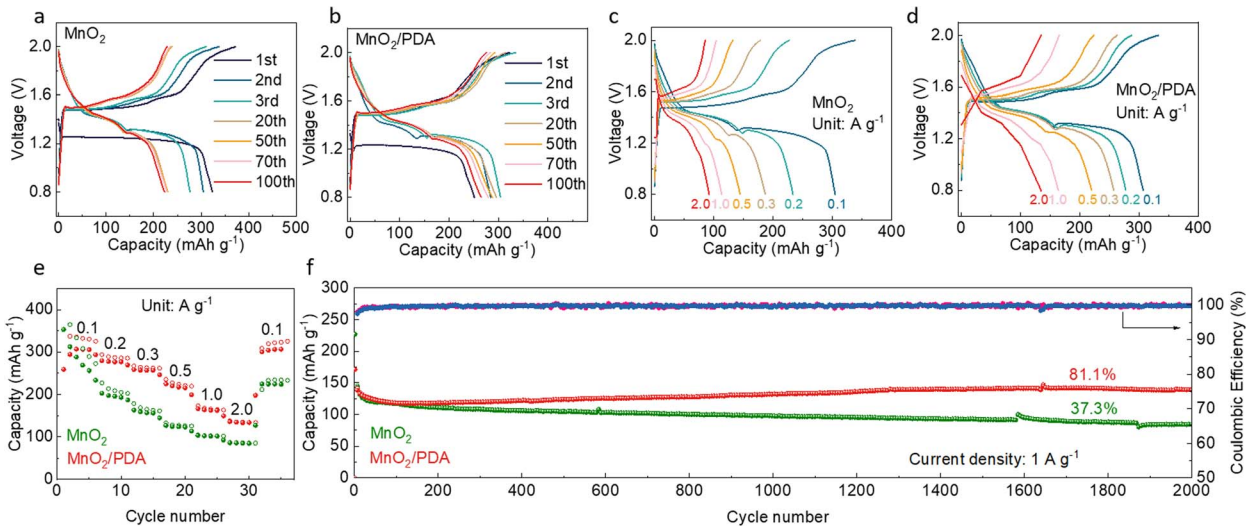

Fig. 2 Electrochemical performance of different cathodes in aqueous zinc batteries with 1 M $ZnSO_4$ electrolyte: charge/discharge curves of (a) MnO_2 and (b) MnO_2/PDA at different cycles at 0.1 A g^{-1}; charge/discharge curves at different current densities of (c) MnO_2 and (d) MnO_2/PDA and (e) their capacities; (f) long-term cycling performance of MnO_2 and MnO_2/PDA at 1 A g^{-1}.

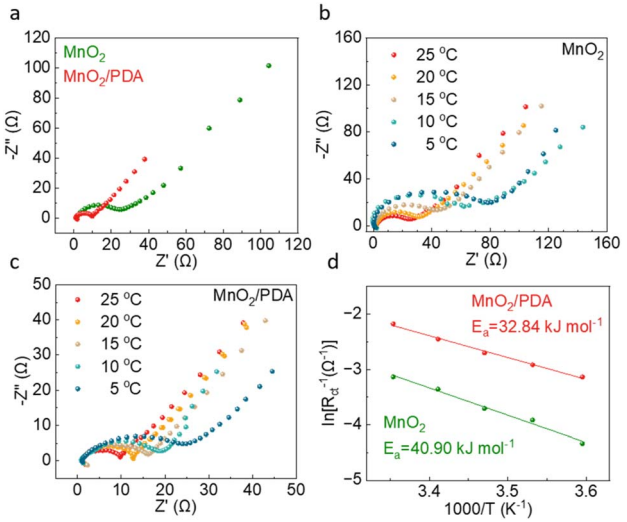

Fig. 3 EIS of MnO_2 and PDA/MnO_2: (a) the comparison of Nyquist plots at 25 °C; the Nyquist plots at various temperatures of (b) MnO_2 and (c) MnO_2/PDA; (d) the linear fits of the $\ln(R_{ct}^{-1})$ *versus* $1000/T$ plots.

hydrogen bonds with protons at the interface with its functional groups such as amino and hydroxyl. This ensures the excellent rate capability of the MnO_2/PDA cathode.

The energy storage mechanisms of the cathodes are studied. Fig. 4a compares the XRD patterns of the MnO_2/PDA cathode at the charged and discharged states. The charged electrode presents diffractions from MnO_2, and extra diffractions from $Zn_4SO_4(OH)_6$ show up upon discharge. Besides, SEM images show nano-rods in the charged cathode and extra flakes are formed during discharge (Fig. 4b and c), which is the typical morphology for basic zinc salts.[41] This suggests proton involved reactions during discharge, including proton intercalation and dissolution processes of MnO_2 based on the following equation: $MnO_2 + 4H^+ + 2e^- = Mn^{2+} + 2H_2O$. The consumption of protons causes a local pH increase and $Zn_4SO_4(OH)_6$ precipitation. The recovery of MnO_2 upon charge confirms a reversible cathode reaction. The nano-rod morphology is still retained after long-term cycling (Fig. S6†). Similar XRD and morphology evolutions are found for the bare MnO_2 cathode (Fig. S7†).

The cycling stability of MnO_2 materials is highly dependent on the active material dissolution/deposition phenomenon. To be more specific, the reduction of MnO_2 during discharge would form Mn^{2+}, which easily dissolves in the electrolyte and causes active material loss. Nevertheless, if they can be reversibly deposited back to the cathode during charge, the active material can be effectively recycled. Meanwhile, this MnO_2/Mn^{2+} reaction is associated with two-electron transfers and adds capacity to the cathode. The above processes are evaluated for the two cathode materials by measuring the Mn concentration changes in the electrolytes at different states by using inductively coupled plasma (ICP, Fig. 4d). With the bare MnO_2 cathode, the Mn concentrations in the electrolyte at the discharged and charged states are 148 mM and 48 mM, respectively. Notably, the Mn in the electrolyte at the charged state corresponds to the active material not able to deposit back,[40] and this irreversible loss of active material results in the fast capacity decay of MnO_2 in zinc cells. With the MnO_2/PDA cathode, on the other hand, lower Mn concentrations are obtained at both states, *i.e.*, 108 mM and 6.5 mM, respectively. This suggests that PDA suppresses Mn^{2+} dissolution during discharge to some extent. Importantly, the low Mn concentration at the charged state demonstrates the reversible oxidation of dissolved Mn^{2+} and its re-deposition as MnO_2 at the cathode. In order to further confirm the positive effect of PDA on Mn^{2+}

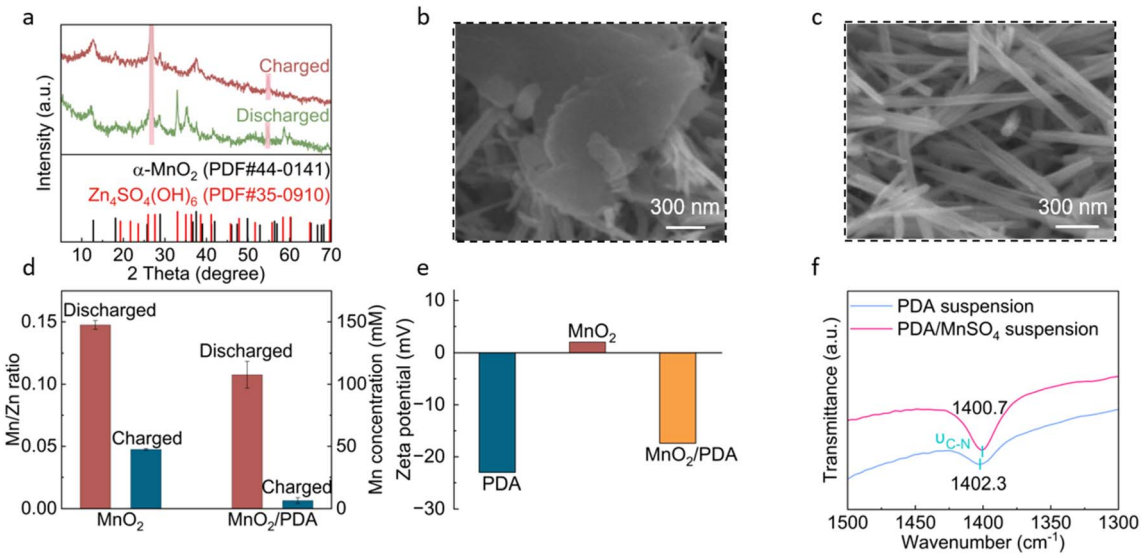

Fig. 4 (a) XRD patterns of the MnO_2/PDA cathode at different states (shaded peaks are from the carbon substrate). SEM images of the (b) discharged and (c) charged MnO_2/PDA cathode. (d) ICP results of Mn/Zn ratios and the calculated Mn concentrations in the 1 M $ZnSO_4$ electrolyte at different states with the MnO_2 and MnO_2/PDA cathodes. (e) The zeta potentials of PDA, MnO_2 and MnO_2/PDA. (f) FT-IR of a PDA suspension in water and $MnSO_4$ solution.

deposition, cells are assembled with cathodes of carbon cloth or carbon cloth coated with PDA (no MnO_2 material) in the electrolyte 1 M $ZnSO_4$ + 0.1 M $MnSO_4$. A constant voltage hold at 2 V is carried out to allow the oxidation of Mn^{2+} in the electrolyte and the deposition of MnO_2 at the cathode. As shown in Fig. S8,† the current response of the carbon cloth electrode decays rapidly and drops below 0.7 mA cm^{-2} after only 30 s. In comparison, the current density of the PDA electrode decays much slower, and it takes 1360 s to drop below 0.7 mA cm^{-2}. The results verify the largely enhanced deposition reaction with the help of PDA. This recycles dissolved active material back to the cathode.

The functioning mechanism of PDA is studied. As discussed earlier in Fig. 1e and f, PDA and MnO_2 exhibit strong coordination interactions. The FT-IR spectra of the MnO_2/PDA cathode at different states show the preservation of PDA vibration peaks (Fig. S9†), suggesting stable interactions during the electrochemical process. We further test the zeta potential of PDA, MnO_2 and MnO_2/PDA (Fig. 4e). The MnO_2 material itself shows a positive zeta potential of around 2 mV, whereas PDA exhibits a negative potential of −23.0 mV. The MnO_2/PDA composite also exhibits a negative value of −17.4 mV. This suggests a negatively charged surface with a PDA component, which provides electrostatic attraction for the dissolved Mn^{2+} cations. Fig. 4f and S10† compare the FT-IR spectra of a PDA suspension in water and $MnSO_4$ solution. Although many vibrations from PDA are overlapped with those of water, the C–N vibration is identified and shows a redshift in $MnSO_4$. This is attributed to the coordination between PDA and Mn^{2+}, confirming their effective interactions. Therefore, although Mn^{2+} are still formed during the discharge process of the MnO_2/PDA cathode, these cations are linked with PDA species and gather around the cathode, resulting in a lower Mn concentration in the bulk electrolyte at the discharged state. Importantly, this strong interaction promotes the re-deposition of Mn^{2+} back to the cathode during the charge process. This retrieves the active material and ensures the stable long-term cycling of the MnO_2/PDA composite material.

Conclusions

In summary, we present a PDA coating strategy to promote the cycling stability of the MnO_2 cathode material in aqueous zinc batteries without relying on pre-added Mn^{2+} salts in electrolytes. FT-IR and Raman results confirm the coordination between nitrogen and oxygen sites on PDA with Mn components, and ICP reveals reduced Mn concentrations in the electrolyte at both discharged and charged states with the MnO_2/PDA composite cathode in comparison to bare MnO_2. This suggests that the strong interactions of PDA with Mn active material effectively confine the latter at the cathode and help the deposition of any dissolved species back to the cathode during the charge process. Therefore, the active material is well maintained for cathode reactions during the electrochemical process, which ensures a stable cycling performance. In aqueous zinc cells with the $ZnSO_4$ electrolyte, the MnO_2/PDA composite cathode retains 147 mA h g^{-1} capacity after 2000 cycles at 1 A g^{-1}. This is superior to the bare MnO_2 material, with only 90 mA h g^{-1} capacity left without the effects from PDA. Our work demonstrates an effective way to promote the cycling performance of manganese oxide electrode materials in aqueous zinc batteries. It could also be applied to other materials with dissolution problems.

Data availability

Data are available from the authors on reasonable request.

Author contributions

G. Z. and X. S. conceived and designed this work. G. Z. carried out the synthesis and electrochemical measurements. All authors participated in the analysis of the data, and discussed and revised the manuscript.

Conflicts of interest

There are no conflicts to declare.

Acknowledgements

This work was supported by the National Natural Science Foundation of China (52174276 and 51974070), the Fundamental Research Funds for the Central Universities (N2105001 and N232410019), and the 111 Project (B16009). Special thanks are due to the instrumental analysis from the Analytical and Testing Center, Northeastern University.

References

1 W. Shang, W. Yu, Y. Liu, R. Li, Y. Dai, C. Cheng, P. Tan and M. Ni, Rechargeable alkaline zinc batteries: Progress and challenges, *Energy Stor. Mater.*, 2020, **31**, 44–57.
2 N. Dong, F. Zhang and H. Pan, Towards the practical application of Zn metal anodes for mild aqueous rechargeable Zn batteries, *Chem. Sci.*, 2022, **13**, 8243–8252.
3 G. Ma, L. Miao, W. Yuan, K. Qiu, M. Liu, X. Nie, Y. Dong, N. Zhang and F. Cheng, Non-flammable, dilute, and hydrous organic electrolytes for reversible Zn batteries, *Chem. Sci.*, 2022, **13**, 11320–11329.
4 J. Shin, J. Lee, Y. Park and J. W. Choi, Aqueous zinc ion batteries: focus on zinc metal anodes, *Chem. Sci.*, 2020, **11**, 2028–2044.
5 Y. Chai, X. Xie, Z. He, G. Guo, P. Wang, Z. Xing, B. Lu, S. Liang, Y. Tang and J. Zhou, A smelting–rolling strategy for ZnIn bulk phase alloy anodes, *Chem. Sci.*, 2022, **13**, 11656–11665.
6 J. S. Lee, S. Tai Kim, R. Cao, N. S. Choi, M. Liu, K. T. Lee and J. Cho, Metal–Air Batteries with High Energy Density: Li–Air *versus* Zn–Air, *Adv. Energy Mater.*, 2011, **1**, 34–50.
7 N. Chang, Y. Yin, M. Yue, Z. Yuan, H. Zhang, Q. Lai and X. Li, A Cost-Effective Mixed Matrix Polyethylene Porous Membrane for Long-Cycle High Power Density Alkaline

Zinc-Based Flow Batteries, *Adv. Funct. Mater.*, 2019, **29**, 1901674.

8 D. Larcher and J. M. Tarascon, Towards greener and more sustainable batteries for electrical energy storage, *Nat. Chem.*, 2014, **7**, 19–29.

9 W. Li, A. Dolocan, P. Oh, H. Celio, S. Park, J. Cho and A. Manthiram, Dynamic behaviour of interphases and its implication on high-energy-density cathode materials in lithium-ion batteries, *Nat. Commun.*, 2017, **8**, 14589.

10 W. Sun, F. Wang, S. Hou, C. Yang, X. Fan, Z. Ma, T. Gao, F. Han, R. Hu, M. Zhu and C. Wang, Zn/MnO_2 Battery Chemistry With H^+ and Zn^{2+} Coinsertion, *J. Am. Chem. Soc.*, 2017, **139**, 9775–9778.

11 M. Yan, P. He, Y. Chen, S. Wang, Q. Wei, K. Zhao, X. Xu, Q. An, Y. Shuang, Y. Shao, K. T. Mueller, L. Mai, J. Liu and J. Yang, Water-Lubricated Intercalation in $V_2O_5{\cdot}nH_2O$ for High-Capacity and High-Rate Aqueous Rechargeable Zinc Batteries, *Adv. Mater.*, 2018, **30**, 1703725.

12 F. Wang, E. Hu, W. Sun, T. Gao, X. Ji, X. Fan, F. Han, X.-Q. Yang, K. Xu and C. Wang, A rechargeable aqueous Zn^{2+}-battery with high power density and a long cycle-life, *Energy Environ. Sci.*, 2018, **11**, 3168–3175.

13 J. Shin, J. Lee, Y. Park and J. W. Choi, Aqueous zinc ion batteries: focus on zinc metal anodes, *Chem. Sci.*, 2020, **11**, 2028–2044.

14 T. Xue and H. J. Fan, From aqueous Zn-ion battery to Zn-MnO_2 flow battery: A brief story, *J. Energy Chem.*, 2021, **54**, 194–201.

15 Y. Zhang, Y. Liu, Z. Liu, X. Wu, Y. Wen, H. Chen, X. Ni, G. Liu, J. Huang and S. Peng, MnO_2 cathode materials with the improved stability *via* nitrogen doping for aqueous zinc-ion batteries, *J. Energy Chem.*, 2022, **64**, 23–32.

16 S. Yang, S. Zhao and S. Chen, Recent advances in electrospinning nanofiber materials for aqueous zinc ion batteries, *Chem. Sci.*, 2023, **14**, 13346–13366.

17 X. Jia, C. Liu, Z. G. Neale, J. Yang and G. Cao, Active Materials for Aqueous Zinc Ion Batteries: Synthesis, Crystal Structure, Morphology, and Electrochemistry, *Chem. Rev.*, 2020, **120**, 7795–7866.

18 Y. Liu, Z. Qin, X. Yang and X. Sun, A Long-Life Manganese Oxide Cathode Material for Aqueous Zinc Batteries with a Negatively Charged Porous Host to Promote the Back-Deposition of Dissolved Mn^{2+}, *Adv. Funct. Mater.*, 2022, **32**, 2106994.

19 G. Fang, J. Zhou, A. Pan and S. Liang, Recent Advances in Aqueous Zinc-Ion Batteries, *ACS Energy Lett.*, 2018, **3**, 2480–2501.

20 P. He, G. Zhang, X. Liao, M. Yan, X. Xu, Q. An, J. Liu and L. Mai, Sodium Ion Stabilized Vanadium Oxide Nanowire Cathode for High-Performance Zinc-Ion Batteries, *Adv. Energy Mater.*, 2018, **8**, 1702463.

21 P. He, Q. Chen, M. Yan, X. Xu, L. Zhou, L. Mai and C.-W. Nan, Building better zinc-ion batteries: A materials perspective, *EnergyChem*, 2019, **1**, 100022.

22 N. Zhang, X. Chen, M. Yu, Z. Niu, F. Cheng and J. Chen, Materials chemistry for rechargeable zinc-ion batteries, *Chem. Soc. Rev.*, 2020, **49**, 4203–4219.

23 V. Mathew, B. Sambandam, S. Kim, S. Kim, S. Park, S. Lee, M. H. Alfaruqi, V. Soundharrajan, S. Islam, D. Y. Putro, J.-Y. Hwang, Y.-K. Sun and J. Kim, Manganese and Vanadium Oxide Cathodes for Aqueous Rechargeable Zinc-Ion Batteries: A Focused View on Performance, Mechanism, and Developments, *ACS Energy Lett.*, 2020, **5**, 2376–2400.

24 J. Li, Y. Chen, J. Guo, F. Wang, H. Liu and Y. Li, Graphdiyne Oxide-Based High-Performance Rechargeable Aqueous Zn–MnO_2 Battery, *Adv. Funct. Mater.*, 2020, **30**, 2004115.

25 H. Pan, Y. Shao, P. Yan, Y. Cheng, K. S. Han, Z. Nie, C. Wang, J. Yang, X. Li, P. Bhattacharya, K. T. Mueller and J. Liu, Reversible aqueous zinc/manganese oxide energy storage from conversion reactions, *Nat. Energy*, 2016, **1**, 16039.

26 J. Huang, Z. Wang, M. Hou, X. Dong, Y. Liu, Y. Wang and Y. Xia, Polyaniline-intercalated manganese dioxide nanolayers as a high-performance cathode material for an aqueous zinc-ion battery, *Nat. Commun.*, 2018, **9**, 2906.

27 M. Zhang, W. Wu, J. Luo, H. Zhang, J. Liu, X. Liu, Y. Yang and X. Lu, A high-energy-density aqueous zinc–manganese battery with a La–Ca co-doped ε-MnO_2 cathode, *J. Mater. Chem. A*, 2020, **8**, 11642–11648.

28 J. Yang, G. Yao, Z. Li, Y. Zhang, L. Wei, H. Niu, Q. Chen and F. Zheng, Highly Flexible K-Intercalated MnO_2/Carbon Membrane for High-Performance Aqueous Zinc-Ion Battery Cathode, *Small*, 2023, **19**, 2205544.

29 X. Shen, X. Wang, Y. Zhou, Y. Shi, L. Zhao, H. Jin, J. Di and Q. Li, Highly Reversible Aqueous Zn-MnO_2 Battery by Supplementing Mn^{2+}-Mediated MnO_2 Deposition and Dissolution, *Adv. Funct. Mater.*, 2021, **31**, 2101579.

30 Z. Li, Y. Li, X. Ren, Y. Zhao, Z. Ren, Z. Yao, W. Zhang, H. Xu, Z. Wang, N. Zhang, Y. Gu, X. Li, D. Zhu and J. Zou, Elucidating the Reaction Mechanism of Mn^{2+} Electrolyte Additives in Aqueous Zinc Batteries, *Small*, 2023, **19**, 2301770.

31 D. Chao, W. Zhou, C. Ye, Q. Zhang, Y. Chen, L. Gu, K. Davey and S. Z. Qiao, An Electrolytic Zn–MnO_2 Battery for High-Voltage and Scalable Energy Storage, *Angew. Chem., Int. Ed.*, 2019, **58**, 7823–7828.

32 T. Xiong, Z. G. Yu, H. Wu, Y. Du, Q. Xie, J. Chen, Y. W. Zhang, S. J. Pennycook, W. S. V. Lee and J. Xue, Defect Engineering of Oxygen-Deficient Manganese Oxide to Achieve High-Performing Aqueous Zinc Ion Battery, *Adv. Energy Mater.*, 2019, **9**, 1803815.

33 Y. Liu, K. Wang, X. Yang, J. Liu, X.-X. Liu and X. Sun, Enhancing Two-Electron Reaction Contribution in MnO_2 Cathode Material by Structural Engineering for Stable Cycling in Aqueous Zn Batteries, *ACS Nano*, 2023, **17**, 14792–14799.

34 Z. He, S. Liu, Y. Zhong, D. Chen, H. Ding, J. Wang, G. Du, G. Yang and Q. Hao, Preparation of BiPO4/graphene photoelectrode and its photoelectrocatalyitic performance, *Chin. J. Catal.*, 2020, **41**, 302–311.

35 J. Yang, D. Chen, Y. Zhu, Y. Zhang and Y. Zhu, 3D-3D porous Bi_2WO_6/graphene hydrogel composite with excellent synergistic effect of adsorption-enrichment and

photocatalytic degradation, *Appl. Catal., B*, 2017, **205**, 228–237.

36 T. Wang, P. Wang, L. Pan, Z. He, L. Dai, L. Wang, S. Liu, S. C. Jun, B. Lu, S. Liang and J. Zhou, Stabling Zinc Metal Anode with Polydopamine Regulation through Dual Effects of Fast Desolvation and Ion Confinement, *Adv. Energy Mater.*, 2023, **13**, 2203523.

37 F. Wu, X. Gao, X. Xu, Y. Jiang, X. Gao, R. Yin, W. Shi, W. Liu, G. Lu and X. Cao, MnO_2 Nanosheet-Assembled Hollow Polyhedron Grown on Carbon Cloth for Flexible Aqueous Zinc-Ion Batteries, *ChemSusChem*, 2020, **13**, 1537–1545.

38 J.-W. Xu, Q.-L. Gao, Y.-M. Xia, X.-S. Lin, W.-L. Liu, M.-M. Ren, F.-G. Kong, S.-J. Wang and C. Lin, High-performance reversible aqueous zinc-ion battery based on iron-doped alpha-manganese dioxide coated by polypyrrole, *J. Colloid Interface Sci.*, 2021, **598**, 419–429.

39 X. Lu, D. Zheng, T. Zhai, Z. Liu, Y. Huang, S. Xie and Y. Tong, Facile synthesis of large-area manganese oxide nanorod arrays as a high-performance electrochemical supercapacitor, *Energy Environ. Sci.*, 2011, **4**, 2915–2921.

40 Y. Liu, Z. Qin, X. Yang, J. Liu, X.-X. Liu and X. Sun, Voltage induced lattice contraction enabling superior cycling stability of MnO_2 cathode in aqueous zinc batteries, *Energy Stor. Mater.*, 2023, **56**, 524–531.

41 Y. Liu, X. Zhou, R. Liu, X. Li, Y. Bai, H. Xiao, Y. Wang and G. Yuan, Tailoring Three-Dimensional Composite Architecture for Advanced Zinc-Ion Batteries, *ACS Appl. Mater. Interfaces*, 2019, **11**, 19191–19199.